Experimental study of microbial induced carbonate precipitation (MICP) in the presence of $CaCO_3$ seeds

Jennifer Zehner,[*,†] Anja Røyne ,[‡] and Pawel Sikorski[†]

†*Department of Physics, Norwegian University of Science and Technology, Trondheim*

‡*The Njord Centre, Department of Physics, University of Oslo, Oslo*

E-mail: jennifer.s.zehner@ntnu.no

Abstract

Microbial-induced calcium carbonate precipitation (MICP) is a biological process inducing bio-mineralization of $CaCO_3$, which can be used to form a solid, concrete-like material. To be able to use MICP successfully for engineering purposes, it is important to understand the formation of the material at the micro-scale to control $CaCO_3$ crystallization. In this contribution we present a systematic study investigating the influence of calcite seeds on the $CaCO_3$ crystallization in MICP. The pH changes during the crystallization process have been monitored in real time with absorption spectroscopy in small volumes, and the optical density (OD) signal was used to analyze the precipitation process. Furthermore, microscopy was used to visualize the precipitation processes in the sample and connect them to changes in pH and OD. We show that there is a significant difference in the pH evolution between samples with and without calcite seeds present and that the shape of the pH evolution and the changes in OD can give valuable information about the precipitation process.

Introduction

Conventional ground improvement techniques are often expensive and have a high impact on the environment[1]. To reduce the environmental impact microbial-induced calcium carbonate precipitation (MICP) can be used for soil stabilization[2,3]. Furthermore, MICP has the potential to replace conventional concrete as a building material in some applications[4]. Conventional concrete production contributes with up to 5% to the anthropogenic CO_2 emissions[5], and therefore there is a strong need for CO_2 reduction within the construction industry. MICP is a biological process based on bio-mineralization that can be used to bind soil particles together, forming so-called bio-concrete. Bio-concrete has the potential to lower the CO_2 emissions in concrete production[6] and is typically based on urea hydrolysis reaction catalyzed by urease enzyme[7,8]:

$$\mathrm{CO(NH_2)_2 + 3\,H_2O \longrightarrow 2NH_4{}^+ + HCO_3{}^- + OH^-} \tag{1}$$

Urea hydrolysis leads to the production of bicarbonate and a pH increase. In the presence of sufficient concentration of calcium ions this can result in $CaCO_3$ precipitation:

$$\mathrm{Ca^{2+} + HCO_3{}^- + OH^- \longrightarrow CaCO_3{\downarrow} + H_2O} \tag{2}$$

Supersaturation is the driving force for precipitation and precipitation can take place once the saturation state in the system $S > 1$[9]:

$$S = \sqrt{\frac{((a_{Ca^{2+}})(a_{CO_3^{2-}}))}{K_{sp}}} \tag{3}$$

where $a_{Ca^{2+}} \cdot a_{CO_3^{2-}}$ is the ion activity product of calcium and carbonate ions in the solution, and K_{sp} is the solubility product of the nucleating polymorph of $CaCO_3$. A sufficient level of supersaturation results in nucleation and is followed by subsequent crystal growth. In MICP processes the supersaturation is controlled by the pH value, the amount of dissolved

inorganic carbon and the calcium concentration[8].

The presence of surfaces in the crystallization solution can lower the energy barrier necessary for nucleation and increase the nucleation rate[10]. This nucleation process is referred to as heterogeneous nucleation. In the MICP process, several injections of crystallization solution are used to achieve sufficiently consolidated granular material[11]. During initial injections calcite crystals will nucleate within the granular medium. Therefore, not only the granular medium, the bacteria cells, and gas bubbles in the system, but also calcite crystals need to be considered as nucleation sites for heterogeneous nucleation.

The suitability of different surfaces as nucleation sites has been investigated previously. Lioliou *et al.*[12] compared nucleation of $CaCO_3$ in the presence of calcite and quartz seeds depending on the supersaturation and showed that lower supersaturation levels are necessary for nucleation and crystal growth for calcite seeds compared to quartz seeds. It was also shown by Dawe *et al.* that gas bubbles in the crystallization system promote $CaCO_3$ precipitation[13]. Furthermore, for MICP the influence of bacteria cell surfaces as nucleation sites has been investigated. While Mitchell *et al.* showed that bacteria surfaces are not good nucleation sites[14], it has been shown recently by Ghosh *et al.* that nanoscale calcium carbonate crystals can be formed on the surface of *Sporosarcina pasteurii*[15]. *S. pasteurii* is an extensively studied microorganism for MICP processes[7,16,17].

We have previously reported an experimental method using absorption spectroscopy to study the precipitation process and the real time pH evolution of MICP without calcite seeds in small volumes[18]. Due to small volumes, mixing and transport occurred by diffusion. For the crystallization without the presence of calcite crystals three stages could be identified. In the first stage, urea hydrolysis catalyzed by bacterial urease increased the pH, and during this phase precipitation of metastable amorphous calcium carbonate (ACC) and vaterite was observed (Stage I). Once the supersaturation reached a critical level nucleation of calcite was observed (Stage II). Nucleation and crystal growth of calcite resulted in a pH decrease (Stage III), while the metastable ACC/vaterite was observed to dissolve.

To be able to understand, predict and control $CaCO_3$ precipitation in MICP processes it is important to understand how the presence of calcite crystals will influence the crystallization. In this contribution we investigated the influence of calcite seeds on the crystallization process in MICP. We compared the precipitation in samples with and without calcite seeds and investigated the precipitation kinetics by monitoring the pH evolution in small volumes with absorption spectroscopy. From the changes in the optical density of the reaction solution, we determine the onset of the precipitation and follow phase transformations. We show that the pH evolution is significantly different between unseeded and seeded samples and can give valuable information about the precipitation process. Furthermore, we demonstrate that precipitation of ACC and vaterite can also occur for samples with calcite seeds present and that that process depends on the bacteria concentration and consequently on the urease activity.

Material and methods

All solutions were filtered with a polycarbonate (0.22 µm) syringe filter before use. The used chemicals were purchased at SigmaAldich (Norway), unless otherwise stated. For preparation of the crystallization solution as well as for the bacteria culture, the same protocol as in previously presented work has been used[18], and a short description of the used protocols is given below.

Crystallization solution

The crystallization solution for the presented experiments consisted out of two components: urea, and dissolved chalk solution. The initial concentration of urea before the start of the hydrolysis reaction was 0.1 M. Dissolved chalk solution (DCS) was used as a calcium source for MICP experiments. Crushed limestone (Franzefoss Miljøkalk AS (Norway)) was dissolved with 300 mM lactic acid. After 24 h reaction time the undissolved parts of the

crushed limestone were filtered out with a 0.22 µm syringe filter. Urease producing bacteria cells were added to the crystallization solution to catalyze the hydrolysis reaction. The amount of the bacteria dilution contributed with 10% to the final volume of the sample.

Bacteria culture

For the presented experiments the urease-producing bacterium *Sporosarcina pasteurii* (Strain DSM33 of *S. pasteurii*) purchased from "Deutsche Sammlung von Mikroorganismen and Zellkulturen" (DSMZ) was used. DSMZ medium 220 with pH of 7.3 supplemented with urea and consisting of $15\,\mathrm{g\,l^{-1}}$ peptone from casein, $5\,\mathrm{g\,l^{-1}}$ peptone from soy meal, $5\,\mathrm{g\,l^{-1}}$ NaCl and $20\,\mathrm{g\,l^{-1}}$ urea was used as growth medium. The culture was inoculated with 1% frozen glycerol stock. After inoculation the culture was incubated overnight (17 h) at 30 °C with constant shaking. Afterward the culture was incubated without shaking at 30 °C until further use 24 h after inoculation. The cultures were prepared for the experiment by centrifuging the culture at $4800 \times g$ for 8 min and the cells were subsequently washed twice with pre-warmed 0.01 M PBS (phosphate buffered saline) to remove the growth medium. The cells were re-suspended and diluted with 0.01 M PBS. Three different bacteria cultures were used for the presented experiments. As an indication of bacterial cell concentration the optical density (OD_{600nm}) at 600 nm was measured in a 96-well plate (volume: 150 µm) before adding the bacteria suspension to the crystallization solution. The optical densities for the bacterial suspensions used in the presented experiments as well as the used sample names are shown in Table 1.

The dilution of the original cultures with PBS is shown in Table S1, Supplementary Information. The optical density values of bacteria cultures given in Table 1 refer to the OD_{600nm} of the bacteria culture before adding the bacteria cells to the crystallization solution.

Table 1: Bacteria cell concentrations of the cultures added to the crystallization solution. The table shows the name and the OD_{600nm} of the bacteria dilutions, which were added to the crystallization solution. The ratio of bacteria dilution to sample volume was 1 to 10. Additionally, the table gives an overview of the sample names, which were used for unseeded and seeded sample where the bacteria dilutions have been added.

Dilution name	**OD_{600nm}**	**Bacteria culture**	**sample name**	
pH monitoring experiments			unseeded	seeded
D1-C1	1.3975	culture1	D1-$C1_{us}$	D1-$C1_s$
D2-C1	1.2967	culture1	D2-$C1_{us}$	D2-$C1_s$
D3-C1	1.1079	culture1	D3-$C1_{us}$	D3-$C1_s$
D4-C1	0.6417	culture1	D4-$C1_{us}$	D4-$C1_s$
Optical microscope experiments			unseeded	seeded
D2-C2	0.8783	culture2	—-	D2-$C2_s$
D1-C3	0.8922	culture3	D1-$C3_{us}$	—-
Confocal laser scanning microscope			unseeded	seeded
D1-C2	0.956	culture2	—-	D1-$C2_s$

Calcite seeds

Calcite seeds for optical microscope and global pH monitoring experiments were prepared by mixing 0.2 M $CaCl_2$ solution with 0.2 M Na_2CO_3 solution in an airtight reactor. The crystallization reaction was performed at 10 °C and the solution was stirred with a mechanical stirrer for 48 h. After the reaction was completed, the calcite seeds were washed with water and ethanol before further use. The finished calcite seeds have been characterized with scanning electron microscopy. The calcite seeds had a rhombohedral shape with a width of about 8 µm (see Supplementary Information: Figure S1).

Additionally, for confocal laser scanning microscope experiments a fluorescent dye was incorporated in the calcite seeds during the crystal growth, following a procedure reported by Green *et al.*[19]. The fluorescent calcite seeds were directly grown on glass microscope cover-slides, as follows: The slides were placed in a beaker with $CaCl_2$ solution and 0.1 mM solution of the fluorescent dye HPTS (8-Hydroxypyrene-1,3,6-trisulfonic acid). To initiate the crystallization, Na_2CO_3 solution was added and mixed thoroughly. The concentration of Ca^{2+} and ${CO_3}^{2-}$ was 5 mM. The reaction was left to proceed for 3 days. Afterwards, the

slides were washed with DI water and ethanol before use. The shape of the crystals with fluorescent dye incorporated are shown in Figure S2, Supplementary Information.

Real time pH monitoring

Real time pH evolution measurements were performed with a method reported earlier to measure the average pH in small volumes (200 µL)[18]. Crystallization solution and the pH indicator Phenol Red (0.4 µM) were pre-mixed in a 96-well plate, and bacteria suspensions were added to start the reaction. To minimize the gas exchange with the environment the well plate was covered with a transparent tape before the measurement was started. The change in the optical density (OD) at 558 nm and 750 nm was measured with a spectrophotometer (SpectraMax® i3 Platform). No signal from the pH sensitive dye was detected above 600 nm, meaning that the change in OD at 750 nm (OD_{750nm}) was only caused by scattering of precipitates, seeds and bacteria cells in the sample. Consequently, the OD_{750nm} could be used for background corrections for the OD at 558 nm. The background corrected OD at 558 nm corresponds to the absorbance of the sample, and the absorbance was used to calculate the pH, using a standard-curve created by recording the background corrected OD for calibration buffers with known pH. The OD_{750nm} was also used to monitor the changes in amount of $CaCO_3$ in the sample, since the change in the OD_{750nm} due to bacterial growth is expected to be small compared to the change due to the precipitation of $CaCO_3$.

Optical microscopy

The crystallization process with and without calcite seeds was monitored with an optical microscope (Motic, AE31E). The crystallization reaction was performed in a 96-well plate (sample volume: 200 µL). The objectives used were 10x (0.25 NA) for crystallization without seeds, and 20x (0.3 NA) for crystallization with seeds. Higher magnification was used for the seeded samples due to the small size of the calcite seeds. Images were recorded with a Moticam 5.0. Optical microscope images were used to estimate how much of the micro-well

bottom was covered with calcite crystals at the end of the experiment. For that purpose, a gray scale threshold value was applied to mask optical microscope images for each sample at different position of the well and the average number of black pixels corresponded to the area of the micro-well bottom which was covered with crystals. An example of the mask applied to a micrograph of one unseeded and one seeded sample is shown Figure S3, Supplementary Information.

Confocal laser scanning microscopy

A confocal laser scanning microscope (CLSM, Leica TCS SP5) using an Argon laser (488 nm) and detection range 500 nm to 550 nm was used to investigate the crystal growth in the presence of fluorescent calcite seeds described above.

Results

Unseeded experiments

The pH evolution as well as the OD_{750nm} curves for $CaCO_3$ precipitation induced by hydrolysis of urea by *S. pasteurii* in samples that did not contain calcite seeds are shown in Figure 1a,b. Experiments were performed using four different bacteria cell concentrations as specified in Table 1.

As expected, the rate of the pH increase at the beginning of the reaction was correlated to the bacterial cell concentration and therefore to the urea hydrolysis rate (Figure 1a). The highest pH was reached for the samples that contained the highest bacterial cell concentration. After a short period of stable pH, the pH decreased and this trend was observed for all four tested bacterial cell concentrations. The pH remained stable longer for lower bacterial cell concentrations. Furthermore, it could be observed that the pH increased in the final stage of the reaction before stabilizing.

The observed changes in the pH of the crystallization solution were correlated with

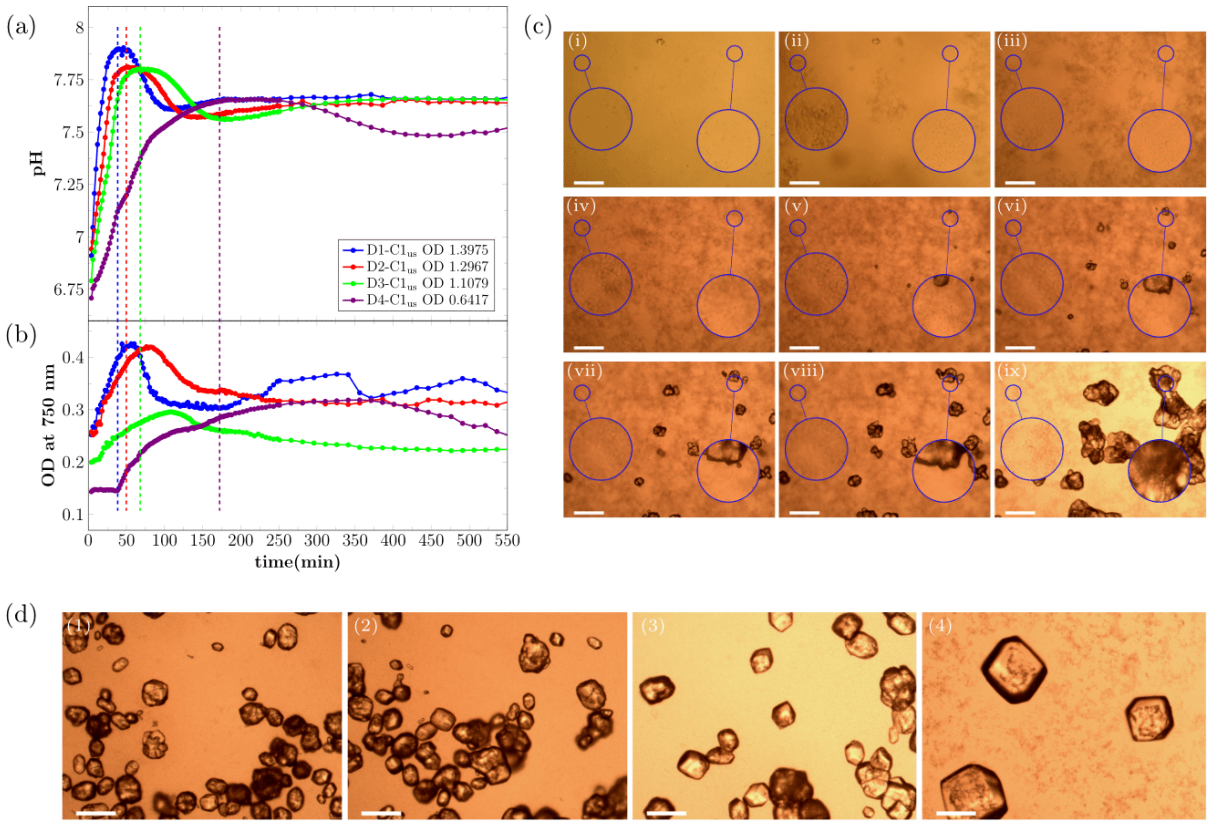

Figure 1: Real time evolution of (a) pH and (b) OD_{750nm} for MICP experiments without the presence of calcite seeds for the first 550 min of the reaction. Note that the first shown data point of the measurement is taken 4 min after the start of the reaction (= 0 min). The signal of the OD_{750nm} correlates with the amount of $CaCO_3$ in the sample. Dashed vertical lines mark the time-point of maximum pH. The OD in the legend shows the OD_{600nm} of the bacteria dilution before adding to the crystallization solution. (c) Optical microscope time-series of precipitation process for bacteria dilution D1-C3 (OD_{600nm}=0.8922) without calcite seeds present for different time-points of the reaction: (i) 0 min, (ii) 14 min, (iii) 23 min, (iv) 47 min, (v) 54 min, (vi) 88 min, (vii) 148 min, (viii) 240 min, and (ix) 21 h. The magnified area on the left shows an area where no calcite will nucleate during the experiment. The magnified area on the right shows an area where a calcite crystal will nucleate. (d) Micrographs of precipitated crystals after 21 h reaction time for (1) D1-$C1_{us}$, (2) D2-$C1_{us}$, (3) D3-$C1_{us}$, and (4) D4-$C1_{us}$ without the presence of calcite seeds. The scale-bar in (c) and (d) is 150 µm.

changes in OD_{750nm}, which measures how much light is scattered by the sample. For the two highest bacteria cell concentrations, the OD_{750nm} increased fast from the beginning of the reaction and decreased after the maximum pH was reached in the sample. For the two lowest bacteria cell concentrations, the OD_{750nm} was nearly stable at the beginning of the reaction, before increasing after 14 min and 38 min for D3-$C1_{us}$ and D4-$C1_{us}$, respectively.

The increase in the OD_{750nm} during the first phase of the reaction can be interpreted as precipitation of amorphous calcium carbonate (ACC), which quickly transformed into vaterite[18]. This was followed by the nucleation of calcite, accompanied by the dissolution of ACC/vaterite. The dissolution of the initially precipitated phase resulted in a decrease of the OD_{750nm} for all four bacteria cell concentrations, as a result of fewer, larger crystals scattering less light than many, small particles. The pH of the sample started to decrease once calcite nucleated. See discussion and Figure 4 for more detailed description of the various processes taking place during precipitation. The second period of pH increase started at the same time as the OD_{750nm} signal started to stabilize. This was most likely caused by a slowing of the calcite precipitation rate due to a low amount of calcium remaining in solution.

This interpretation is supported by optical microscopy. Figure 1c shows selected time-points for the precipitation reaction for the sample D1-$C3_{us}$ (see Table 1). The precipitation of small particles was observed in the initial stage of the reaction (Figure 1c, i-iv). These precipitates have been characterized previously[18] and identified as ACC, which quickly transforms into vaterite. After the nucleation of calcite crystals (Figure 1c, v), the calcite crystals grew and the ACC/vaterite phase dissolved. The dissolution was fastest near existing calcite crystals (Figure 1c,v-viii, magnified area on the right).

Figure 1d shows crystals precipitated in the experiments described above (Figure 1a,b) imaged after the reaction was completed (21 h). It was observed that the bacteria cell concentration had a significant effect on the morphology of the precipitated crystals. For the highest bacteria cell concentration (D1-C1) the smallest crystals, with a mixture of rhombohedral and spherical morphology were observed (Figure 1d,1). For samples with

lower bacteria cell concentration, the precipitated crystals were larger and had a more regular rhombohedral shape (Figure 1d, 2-4)).

Optical microscope images (Figure 1d) were also used to estimate the fraction of the micro-well bottom covered with calcite crystals at the end of the experiment (see Materials and Methods). The observed amount of precipitation followed the same trend as the sample OD when plotted against the starting concentration of the bacteria, see Figure S4a, Supplementary Information. A higher starting concentration of bacteria cells resulted in a larger amount of smaller crystals. Those covered a larger area of the well-bottom compared to a low bacteria cell starting concentration where the precipitated crystals covered a smaller area of the well bottom. The same trend was observed for the OD_{750nm}. A larger number of small crystals resulted in a higher signal of the OD_{750nm} compared to fewer and bigger crystals. Therefore, the OD_{750nm} could be used to give an estimate of the fraction of the micro-well bottom, which was covered with $CaCO_3$ crystals, as well as for an estimate the onset of precipitation and transformations.

Seeded samples

The presence of calcite seeds had two effects on the MICP (Figure 2a,b). First, the seeds affected the pH of the crystallization solution before the onset of the urea hydrolysis reaction, due to partial dissolution of the calcite seeds in the initially undersaturated solution. The starting pH was around 5.3 for unseeded and 6.1 for seeded samples (see Table S2, Supplementary Information). Secondly, seeds affected the precipitation process as the calcite seeds acted as nucleation sites for heterogeneous nucleation.

As for the unseeded samples, the pH increase at the beginning of the reaction was correlated to the bacterial cell concentration (Figure 2a). The period of rapid pH increase was followed by a pH decrease for the three highest bacteria cell concentrations. For the lowest bacteria cell concentration, no pH decrease was observed, and the pH stabilized after the initial pH increase.

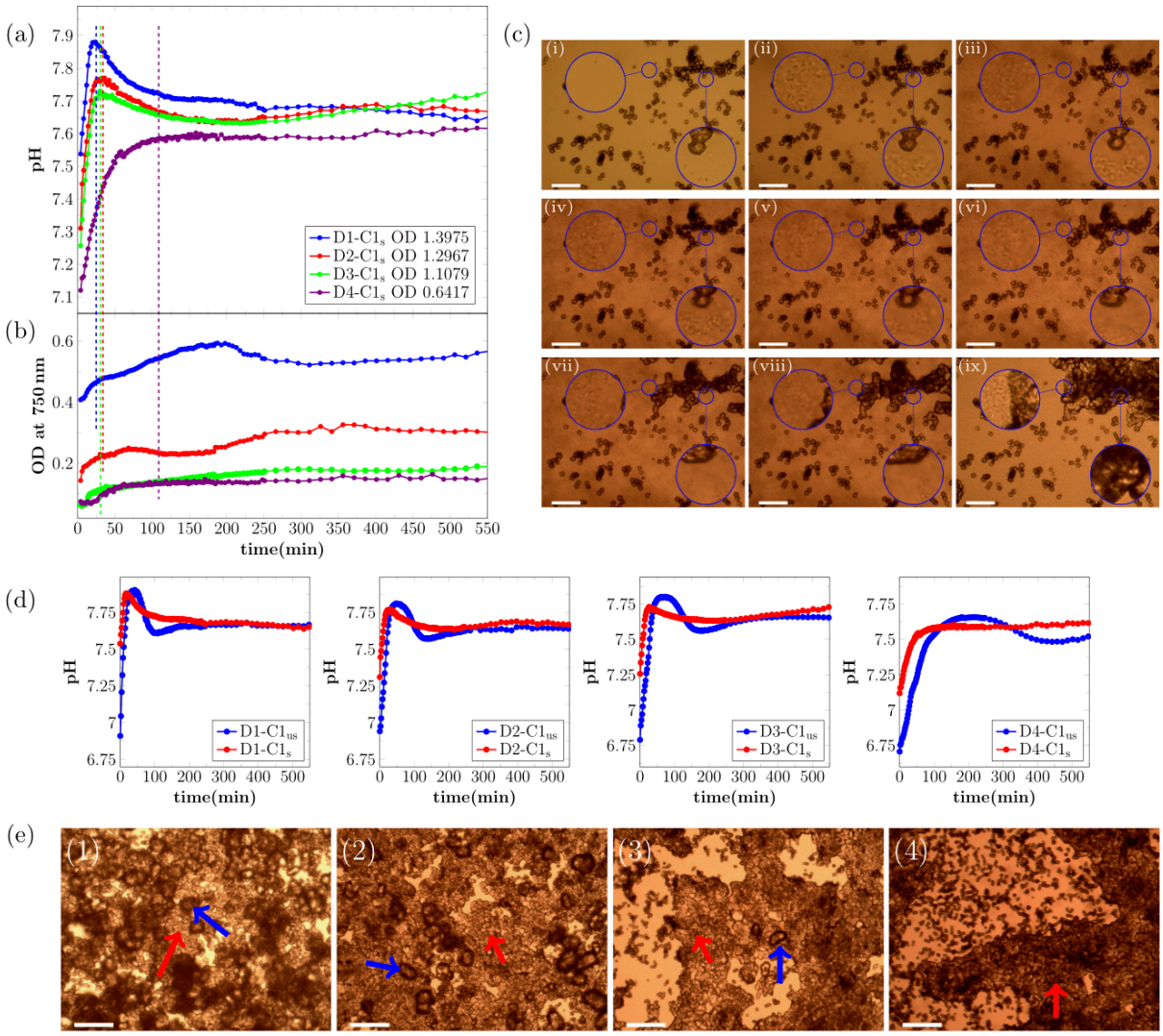

Figure 2: Real-time evolution of (a) pH and (b) OD_{750nm} for MICP experiments with the presence of calcite seeds. Note that the first shown data point of the measurement is taken 4 min after the start of the reaction. The OD_{750nm} was measured before start of the reaction to get the contribution of the initial seeds in the crystallization solution, and this starting value was subtracted form the OD_{750nm}. Therefore, the shown signal is correlated to the amount of precipitated $CaCO_3$. The OD in the legend shows the OD_{600nm} of the bacteria dilution before adding to the crystallization solution. (c) Optical microscope time-series of the precipitation process for bacteria dilution with OD_{600nm}=0.8783 with calcite seeds present for different time-points of the reaction: (i) 0 min, (ii) 20 min, (iii) 28 min, (iv) 50 min, (v) 80 min, (vi) 110 min, (vii) 170 min, (viii) 230 min, and (ix) 21 h. The magnified area on the right shows calcite seeds, which will increase in size during the experiment. The magnified area on the left shows an area with a small distance to calcite seeds which will increase in size during the experiment. (d) Comparison of real time pH evolution of MICP experiments with and without calcite seeds. (e) Micrographs of precipitated crystals after 21 h reaction time for (1) D1-$C1_s$, (2) D2-$C1_s$, (3) D3-$C1_s$, and (4) D4-$C1_s$. The red arrows indicate calcite seeds which grew during the experiment and the blue arrows indicate additional nucleated calcite crystals. The scale-bar is 50 µm in (c) and 150 µm in (e).

As seen in Figure 2d, the shape of the pH curves is different for unseeded and seeded samples. The pH increase curve had approximately the same slope for both unseeded and seeded samples at the start of the reaction. The offset along the time axis between unseeded and seeded pH curves was caused by the higher starting pH of the seeded samples (see Table S2, Supplementary Information). The maximum reached pH was lower for the seeded samples. This was probably caused by an onset of nucleation and crystal growth at lower supersaturation levels due to the existing calcite surfaces. For the three highest bacteria cell concentrations, the pH decrease was faster for unseeded than for seeded samples. The second pH increase was much more pronounced for the unseeded samples (Figure 2d).

The OD_{750nm} of the seeded samples was measured before adding the bacteria cells, and this value was subtracted from the subsequent OD_{750nm} measurement to ensure the OD_{750nm} signal shown in Figure 1b does not include the contribution of the calcite seeds. Changes in the sample OD_{750nm} in Figure 1b were therefore mainly caused by the precipitation of $CaCO_3$. For the two highest bacteria cell concentrations, the OD_{750nm} of the samples increased throughout the reaction. For the two lowest bacteria cell concentrations, the OD_{750nm} of the sample was constant at the beginning of the reaction and started to increase after 14 min and 28 min for D3-$C1_s$ and D4-$C1_s$, respectively. The increase in OD_{750nm} was observed for both samples only during the pH increase in the initial phase of the reaction.

The precipitation process for the sample D2-C2 (see Table 1) was investigated with optical microscopy (Figure 2c) to correlate changes in the OD_{750nm} to changes in $CaCO_3$ morphology. Similar to the unseeded experiments, precipitation of small particles was observed in the initial phase of the reaction (Figure 2c, ii-iii). The morphology of the precipitated particles was similar to what was observed in the unseeded experiments and therefore the initial precipitation could be identified as ACC/vaterite. The precipitation of ACC/vaterite was also indicated by a change in the OD_{750nm} of the samples during the initial reaction stage. The initial precipitation of ACC/vaterite was followed by growth of the crystal seeds present in the sample (Figure 2c, iv-ix), and the ACC/vaterite dissolved at the later stage of the reaction

(see magnified areas in Figure 2c, v-vii) with faster dissolution in close proximity of the growing crystals (magnified area on the right). The dissolved ACC/vaterite reprecipitated on the surface of the seeds, but no pronounced decrease in the OD_{750nm} was observed, most likely due to the fact that less calcium was bound in metastable precipitates in seeded samples.

For the two lowest bacteria cell concentrations, the onset of precipitation occurred earlier in the seeded than in the unseeded experiments. This is likely a consequence of the higher starting pH of the crystallization solution, due to partly dissolved calcite seeds (Table S2, Supplementary Information).

Optical micrographs of crystals precipitated in seeded experiments recorded after 21 h are shown in Figure 2e. For a low hydrolysis rate, only the growth on calcite seeds was observed in the sample (red arrow in Figure 2e, 4). However, for the three highest bacteria cell concentrations, which corresponded to a higher hydrolysis rate, additional nucleated calcite crystals were observed in the samples. The additional nucleated crystals are marked with a blue arrow and calcite seeds which increased in size during the reaction are marked with a red arrow (Figure 2e, 1-3). The additional precipitated calcite crystals in Figure 2e had a more irregular shape compared to samples without calcite seeds present Figure 2.

The growth process on the surface of the calcite seeds was investigated in more detail with confocal laser scanning microscopy (Figure 3a-f). The growth process is shown for 6 time-points. Figure 3a shows the calcite seed 1 min before the crystal growth started. The crystal growth on the surface of the calcite seed started with small islands on the calcite crystal (Figure 3b) and the islands increased in size over the 13 min (Figure 3c-e), until the growing crystals formed a new layer of calcite on the surface of the calcite seed (Figure 3f). The incorporation of a fluorescent dye into the calcite seed crystal made it possible to distinguish between the crystal seeds and the newly grown crystals (Figure 3g).

From the optical images collected after 21 h (Figure 2d) we estimated the fraction of the sample well that was covered with calcite crystals at the end of the reaction (see Materials and

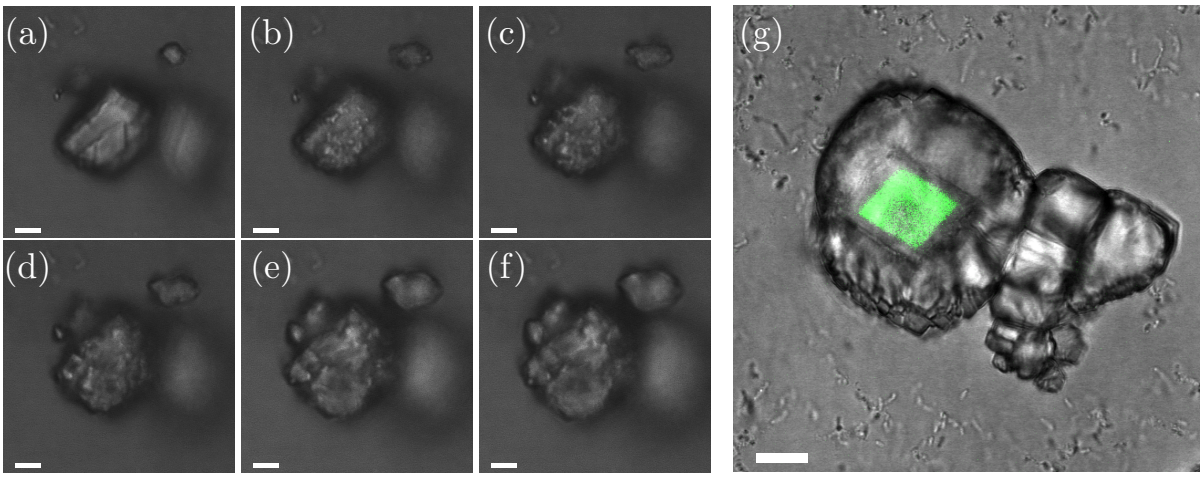

Figure 3: (a-f) Growth process of calcite seeds. Images are taken with a CLSM. Images are taken (a) 1 min before the growth process started, and (b) 1 min (c) 3 min (d) 6 min, (e) 11 min and (f) 14 min after the growth process started. (g) Finished crystal. The original fluorescent calcite seed had a fluorescent dye incorporated and was visualized with CLSM.

Methods). Figure S4b, Supplementary Information, shows how the amount of precipitation observed in optical microscopy correlates with the OD_{750nm}. Both curves follow the same trend when plotted against the starting concentration of the bacteria cells.

Discussion

In the presented experiments we investigated the influence of calcite seeds on the $CaCO_3$ precipitation in MICP experiments.

We observe differences in the pH evolution for unseeded and seeded samples (Figure 2d). These differences can be connected to different precipitation processes. In the initial phase of the experiment a rapid pH increase was observed for both unseeded and seeded samples. The pH increase was correlated to the urea hydrolysis rate, which was controlled by the bacteria cell concentration. The bacteria cells were washed before the experiments, therefore there was no free enzyme present in the bacteria dilution. However, the used bacteria strain (DSM33) has always urease enzyme with high activity present[20,21], located most likely in the cell membrane. Urea hydrolysis and pH increase started just after adding the bacteria to

the reaction well. The timescale of the experiment was not sufficiently long for the bacteria to produce urease as a response to the presence of urea.

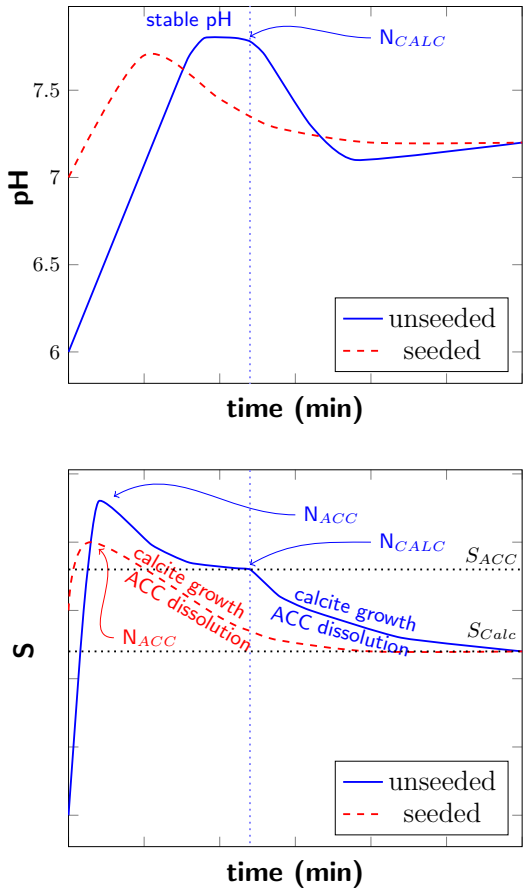

Figure 4: Schematic illustration of real time pH evolution (top) and saturation level (bottom) of unseeded and seeded samples with high bacteria cell concentration. N_{ACC} and N_{CALC} mark the nucleation of ACC and calcite. S_{ACC} and S_{CALC} represent $S = 1$ with respect to ACC and calcite, respectively.

With increasing pH in the samples the saturation level S was increased. The connection between pH evolution and saturation for unseeded and seeded samples for high bacteria cell concentration is schematically shown in Figure 4. For unseeded samples ACC nucleated once S_{ACC} was significantly bigger than 1 and the precipitation of ACC reduced S. Precipitated ACC transforms rapidly to vaterite according to Ostwald's rule of stages (to simplify the process this transformation is not shown in Figure 4). At the point when the stable pH was reached, the urea hydrolysis rate by bacterial urease was equal to the precipitation

rate. The reaction solution was more saturated with respect to calcite than with respect to ACC/vaterite. Once calcite nucleated, it contributed to reducing S due to growth of calcite crystals and resulted in a pH decrease. The solution becomes undersaturated with respect to ACC/vaterite and the metastable phases dissolve. For lower bacteria cell concentrations lower maximum pH values and corresponding lower S were reached. Therefore, a longer stable pH region was observed before the pH started to decrease after calcite nucleation (Figure 1a).

In the seeded samples of the experiments this stable pH region was short and the shape of the pH curves was similar for the three highest bacterial cell concentrations. For the lowest bacterial cell concentration no pH decrease was observed, and the pH stabilized after the initial pH increase (Figure 2a). This could be connected to the precipitation of ACC and calcite in seeded samples. For the three highest bacteria cell concentrations, the pH increased to a value of above 7.7 in the initial phase of the reaction, indicating that growth of calcite seeds was not sufficient to consume hydrolysis products. High pH and corresponding supersaturation resulted in precipitation of ACC also for seeded samples and this is also confirmed by optical microscopy (Figure 2c). The pH decrease that is observed after the maximum pH is reached is a consequence of nucleation of new calcite crystals and crystal growth. The initial calcite seeds acted as nucleation sites, and therefore no significant time-delay of nucleation was observed for the three highest bacterial cell concentrations. Calcite growth was responsible for reducing the supersaturation and the pH and ACC/vaterite dissolved (see Figure 4). For the lowest bacterial cell concentration no pH decrease was observed, most likely due to the fact that supersaturation produced by urea hydrolysis was reduced by growth of existing calcite seeds.

Calcite nucleated at lower pH values for seeded samples (Figure 2d) and therefore at lower supersaturation. The influence of calcite seeds on $CaCO_3$ precipitation in non-MICP experiments was reported earlier, and it was shown, that in the presence of calcite seeds, $CaCO_3$ nucleation can take place at lower supersaturation levels[12,22]. In our experiments,

we could confirm this also for MICP experiments.

Furthermore, it was observed for unseeded samples that the bacterial cell concentration had a strong influence on the size and shape of the precipitated calcite crystals. It has been reported previously that a high supersaturation condition for nucleation leads to smaller $CaCO_3$ crystal sizes[23]. Cheng *et al.* and Cuberth *et al.* reported that the initial ureolysis rate in MICP experiments influenced the crystal size[24,25]. Wang *et al.* showed recently that the urease activity is increased with higher bacteria density and that higher bacteria densities in MICP experiments resulted in a high nucleation rate, due to the precipitation of unstable phases of $CaCO_3$[26]. This was also observed in our experiments (Figure 1d). The higher ureolysis rate in the beginning of the experiment resulted in a larger amount of ACC/vaterite precipitation, which could act as nucleation sites for calcite crystals. This resulted in the nucleation of a larger number of smaller crystals.

Furthermore, we observed the precipitation of ACC/vaterite in seeded samples (Figure 2). ACC/vaterite precipitation was reported earlier for unseeded samples[18,27]. However, we were able to show by comparing unseeded to seeded experiments that the metastable polymorph phases can also precipitate for samples where calcite seeds were present (Figure 2). The presence of calcite seeds lowered the energy barrier for nucleation, resulting in lower pH values were necessary for calcite nucleation. However, the presence of calcite seeds did not suppress the formation of metastable phases for higher bacteria cell concentrations.

Conclusions

We presented a systematic study investigating the influence of calcite seeds on the crystallization processes of $CaCO_3$ in MICP experiments. In our experiments we observed a difference in the pH evolution between unseeded and seeded experiments, caused by different crystallization processes of $CaCO_3$. Lower pH values were necessary for calcite nucleation in seeded experiments. Furthermore, by analyzing the real time pH evolution and OD_{750nm}

we could detect the precipitation of the metastable phases of ACC/vaterite also for samples with calcite seeds present.

The production of MICP materials is often based on several injections of the crystallization solution in the granular medium, and after the first injections calcite crystal will be present in the system and have to be considered as additional nucleation sites for $CaCO_3$ precipitation. The results obtained in this study show that calcite crystals in the system will influence the $CaCO_3$ precipitation. Also the precipitation of metastable polymorph phases has to be considered in the production process of MICP materials. The understanding of those processes is important to be able to control and predict $CaCO_3$ precipitation within a granular medium and to produce a sustainable, solid, and concrete-like material.

Acknowledgement

This work was supported by the Research Council of Norway under project 269084/O70. Additional support was provided by Norwegian Micro- and Nano-Fabrication Facility, NorFab under Research Council of Norway project 245963/F50. The authors thank Simone Balzer Le from SINTEF Industry, Trondheim, Norway, for providing the bacteria cultures for the performed experiments and Seniz Ucar from the department of Chemical Engineering, NTNU, Trondheim, Norway for the fabrication of the calcite seeds.

Supporting Information Available

The supporting information includes:

- Table S1: Dilution table of bacterial cultures
- Table S2: Initial pH values of seeded and unseeded samples
- Figure S1: SEM images of calcite seeds

- Figure S2: Confocal laser scanning microscope image of fluorescent calcite seeds
- Figure S3: Example of masking optical micrographs for unseeded and seeded experiments
- Figure S4: Comparison between OD_{750nm} signal at the end of the measurement and percentage of bottom of the micro-well covered with calcite crystals.

References

(1) Ivanov, V.; Chu, J. Applications of microorganisms to geotechnical engineering for bioclogging and biocementation of soil in situ. *Reviews in Environmental Science and Bio/Technology* **2008**, *7*, 139–153.

(2) Whiffin, V. S.; Van Paassen, L. A.; Harkes, M. P. Microbial carbonate precipitation as a soil improvement technique. *Geomicrobiology Journal* **2007**, *24*, 417–423.

(3) DeJong, J. T.; Fritzges, M. B.; Nüsslein, K. Microbially induced cementation to control sand response to undrained shear. *Journal of Geotechnical and Geoenvironmental Engineering* **2006**, *132*, 1381–1392.

(4) De Muynck, W.; De Belie, N.; Verstraete, W. Microbial carbonate precipitation in construction materials: a review. *Ecological Engineering* **2010**, *36*, 118–136.

(5) Le Quéré, C.; Moriarty, R.; Andrew, R. M.; Canadell, J. G.; Sitch, S.; Korsbakken, J. I.; Friedlingstein, P.; Peters, G. P.; Andres, R. J.; Boden, T. A., et al. Global carbon budget 2015. *Earth System Science Data* **2015**, *7*, 349–396.

(6) Myhr, A.; Røyne, F.; Brandtsegg, A. S.; Bjerkseter, C.; Throne-Holst, H.; Borch, A.; Wentzel, A.; Røyne, A. Towards a low CO2 emission building material employing bacterial metabolism (2/2): Prospects for global warming potential reduction in the concrete industry. *PloS one* **2019**, *14*.

(7) Stocks-Fischer, S.; Galinat, J. K.; Bang, S. S. Microbiological precipitation of CaCO3. *Soil Biology and Biochemistry* **1999**, *31*, 1563–1571.

(8) Hammes, F.; Verstraete, W. Key roles of pH and calcium metabolism in microbial carbonate precipitation. *Reviews in Environmental Science and Biotechnology* **2002**, *1*, 3–7.

(9) Morse, J. W. The kinetics of calcium carbonate dissolution and precipitation. *Carbonates: Mineralogy and Chemistry, Reviews in Mineralogy* **1983**, *11*, 227–264.

(10) Mullin, J. *Crystallization*; Chemical, Petrochemical & Process; Elsevier Science, 2001.

(11) Røyne, A.; Phua, Y. J.; Le, S. B.; Eikjeland, I. G.; Josefsen, K. D.; Markussen, S.; Myhr, A.; Throne-Holst, H.; Sikorski, P.; Wentzel, A. Towards a low CO2 emission building material employing bacterial metabolism (1/2): The bacterial system and prototype production. *PloS one* **2019**, *14*.

(12) Lioliou, M. G.; Paraskeva, C. A.; Koutsoukos, P. G.; Payatakes, A. C. Heterogeneous nucleation and growth of calcium carbonate on calcite and quartz. *Journal of colloid and interface science* **2007**, *308*, 421–428.

(13) Dawe, R. A.; Zhang, Y. Kinetics of calcium carbonate scaling using observations from glass micromodels. *Journal of Petroleum Science and Engineering* **1997**, *18*, 179–187.

(14) Mitchell, A. C.; Ferris, F. G. The influence of Bacillus pasteurii on the nucleation and growth of calcium carbonate. *Geomicrobiology Journal* **2006**, *23*, 213–226.

(15) Ghosh, T.; Bhaduri, S.; Montemagno, C.; Kumar, A. Sporosarcina pasteurii can form nanoscale calcium carbonate crystals on cell surface. *PloS one* **2019**, *14*.

(16) Achal, V.; Mukherjee, A.; Basu, P. C.; Reddy, M. S. Strain improvement of Sporosarcina pasteurii for enhanced urease and calcite production. *Journal of Industrial Microbiology and Biotechnology* **2009**, *36*, 981–988.

(17) Sarda, D.; Choonia, H. S.; Sarode, D. D.; Lele, S. S. Biocalcification by Bacillus pasteurii urease: A novel application. *Journal of Industrial Microbiology and Biotechnology* **2009**, *36*, 1111–1115.

(18) Zehner, J.; Røyne, A.; Wentzel, A.; Sikorski, P. Microbial-induced calcium carbonate precipitation: an experimental toolbox for in situ and real time investigation of microscale pH evolution. *RSC Adv.* **2020**, *10*, 20485–20493.

(19) Green, D. C.; Ihli, J.; Thornton, P. D.; Holden, M. A.; Marzec, B.; Kim, Y.-Y.; Kulak, A. N.; Levenstein, M. A.; Tang, C.; Lynch, C., et al. 3D visualization of additive occlusion and tunable full-spectrum fluorescence in calcite. *Nature communications* **2016**, *7*, 1–13.

(20) Kaltwasser, H.; Krämer, J.; Conger, W. Control of urease formation in certain aerobic bacteria. *Archiv für Mikrobiologie* **1972**, *81*, 178–196.

(21) Mörsdorf, G.; Kaltwasser, H. Ammonium assimilation in Proteus vulgaris, Bacillus pasteurii, and Sporosarcina ureae. *Archives of microbiology* **1989**, *152*, 125–131.

(22) Tai, C. Y.; Chen, P.-C. Nucleation, agglomeration and crystal morphology of calcium carbonate. *AIChE Journal* **1995**, *41*, 68–77.

(23) Mersmann, A.; Kind, M. Chemical engineering aspects of precipitation from solution. *Chemical engineering & technology* **1988**, *11*, 264–276.

(24) Cheng, L.; Shahin, M. A.; Mujah, D. Influence of key environmental conditions on microbially induced cementation for soil stabilization. *Journal of Geotechnical and Geoenvironmental Engineering* **2017**, *143*, 04016083.

(25) Cuthbert, M. O.; Riley, M. S.; Handley-Sidhu, S.; Renshaw, J. C.; Tobler, D. J.; Phoenix, V. R.; Mackay, R. Controls on the rate of ureolysis and the morphology of car-

bonate precipitated by S. Pasteurii biofilms and limits due to bacterial encapsulation. *Ecological Engineering* **2012**, *41*, 32–40.

(26) Wang, Y.; Soga, K.; DeJong, J. T.; Kabla, A. J. Effects of bacterial density on growth rate and characteristics of microbial-induced CaCO3 precipitates: a particle-scale experimental study. *arXiv preprint arXiv:2007.04094* **2020**,

(27) Zhang, W.; Ju, Y.; Zong, Y.; Qi, H.; Zhao, K. In Situ Real-Time Study on Dynamics of Microbially Induced Calcium Carbonate Precipitation at a Single-Cell Level. *Environmental Science & Technology* **2018**, *52*, 9266–9276.

Synopsis

The influence of calcite seeds was investigated on microbial-induced carbonate precipitation for knowledge-based material improvement of a sustainable construction material.
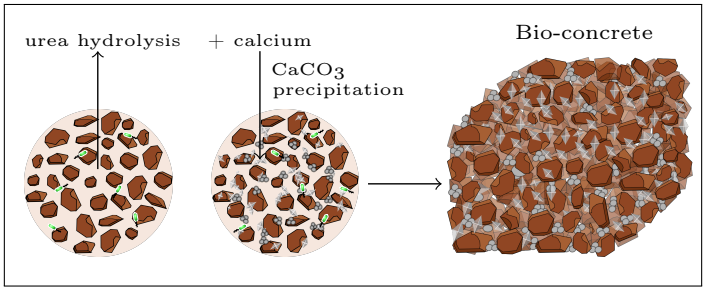
Graphical TOC Entry